Magazine of Civil Engineering

ISSN 2712-8172

journal homepage: http://engstroy.spbstu.ru/

DOI: 10.34910/MCE.105.5

Self-sensing cement composite for traffic monitoring in intelligent transport system

M.T. Bashir*[a,b], M. Daniyal[c], M. Alzara[b], M. Elkady[b], A. Armghan[b]

[a] *CECOS University of IT and Emerging Sciences, Peshawar, Pakistan*

[b] *Jouf University, Sakaka, Al-Jouf, Saudi Arabia*

[c] *Qurtuba University of Science & Information Technology, Department of Civil Engineering, Dera Ismail Khan, Pakistan*

**E-mail: tariqbashir@cecos.edu.pk*

Keywords: granulated blast furnace slag (GGBFS), carbon black (CB), cement-based composites, Piezo resistive properties, traffic monitoring.

Abstract. Self-sensing cement-based composite was used to monitor the flow of traffic volume. Composite material was prepared with numerous percentages of carbon black (CB) and activated granulated ground blast furnace slag (GGBFS). This economical and concrete friendly material having piezo resistive properties helped to detect the wheel pressure induced by the vehicles passing over it. Initially, the pressure sensitivity of different mix designs was investigated in the laboratory and the samples having more sensitivity to applied load were used on the real road test for vehicle detection. Mechanical and microstructural properties of hydrated cement composite filled with CB and GGBFS as an active filler were also explored. Scanning electron microscopy/Electron dispersive spectroscopy (SEM/EDS) and X-ray diffraction (XRD) analysis were carried out to characterize the microstructure and hydration product development of different specimens at different curing ages. The tested cement composite gives a remarkable response to both compressive and vehicular loading with excellent mechanical and microstructural properties. The results also showed that the self-sensitive cement composite has a great potential to use as a device for traffic monitoring.

1. Introduction

Vehicle recognition is one of the critical elements in the management and operation of the traffic system all over the world [1, 2]. At present, various detection systems are used to accumulate and process the traffic data. These traffic data include traffic volume, vehicle speed, vehicle length and width, traffic density that are obtained by sensors either buried beneath the road or operational along the roadside. Until now, many types of detectors are used to detect traffic data. Some of these include electronic, magnetic, video, acoustic devices and optical detectors [1, 2].

Among all these sensors, the electronic sensors are preferably used because they have excellent sensing capability, modern-day technology, resistance to all types of weather conditions and are relatively cheaper in costs. Though these type of sensors can accurately measure the traffic flow data like traffic volume, vehicles speed, vehicles occupancy ratio and weight of vehicles but these type of sensors also have some defects on pavement life due their unfavorable compatibility and bond with pavement structure. Advancement in technology, Microsoft computers, and latest communication systems encourage to introduce the latest technologies for traffic monitoring including infrared sensors, microwave radars, and video image processors but these advanced sensors are facing some limitations such as high manufacturing and maintenance cost, poor performance in faulty weather conditions (fog, smoke, rain, and

Bashir, M.T., Daniyal, M., Alzara, A., Elkady, M., Armghan, A. Self-sensing cement composite for traffic monitoring in intelligent transport system. Magazine of Civil Engineering. 2021. 105(5). Article No. 10505. DOI: 10.34910/MCE.105.5

snow) and so on. Moreover, additional structures and time-consuming calibrations are mandatory to install these type of detectors [3, 4].

In the field of Nano-technology, scientists have presented self-sensing cement based sensors maintaining good mechanical and binding properties of cement, that provides a smart way to detect the traffic flow [5]. These types of sensors are fabricated by filling different conductive materials into the cement to enhance the ability to sense the stress or strain [6]. When the cement composite experiences some kind of load, it is deformed, and the contact between conductive material and cement is effected thus affecting the electrical resistivity of the composite [7, 8]. Vehicle detection sensors constructed with smart cement-based mixtures have many advantages over conventional detectors, such as easy installation, easy maintenance, low cost, useful service life, better compatibility with road structure, as they are cement-based materials [9, 10].

In the past few decades, numerous active materials have been presented for piezo resistive cement-based stress sensors [11]. The first reported material was carbon fiber (CF) which was used in cement to enhance the piezo resistive properties. The relationship between applied load and change in electrical resistance of CF based cement composite was clearly and comprehensively described in the article [6]. To proceed this research, new supplements were introduced and studied including carbon fibers (CF) [10, 12–15], steel fibers (SF) [16–18], carbon nanotubes (CNT) [9, 19–21], carbon black (CB) [22–25], graphene [26, 27], hybrid of carbon black and carbon fiber [24, 25], hybrid of carbon fiber and carbon nanotubes [19]. These supplements were introduced to cement because of their electrical conductivity and piezoresistivety [28–30].

Moreover, Gwen et al., in October 2012, investigated that pozzolanic material (fly ash) with a high content of FeO (15.10 %), when mixed with cement up to 40 % of its weight, gave a reversible response to cyclic compressive loading**.** The workability and economy of cement mortar were also enhanced using magnetic-concentrated fly ash, but a little decrease in compressive and tensile strength was reported due to the high concentration of pozzolanic material [31]. It is noted among all the existing conductive materials, the carbon black when mixed with cement gives mature and even response to compressive loading [22, 32, 33]. Furthermore, carbon black is very cost effective and radially available material throughout the world [24, 34, 35].

2. Materials and Methods

2.1. Materials

The materials used were Portland cement (ASTM C 150), superplasticizer commercially available as acrylic acid ($C_3H_3O_2Zn^+$) was used as water reducing agent, activated (fine up to 99 % having larger surface area) granulated ground blast furnace slag (FeO concentrated) [31], Carbon black with arbanion ions (Type N-550) (Table 1 & 2) and galvanized #6 steel meshes (opening of 4.2 mm) were used as electrodes shown in Fig. 1.

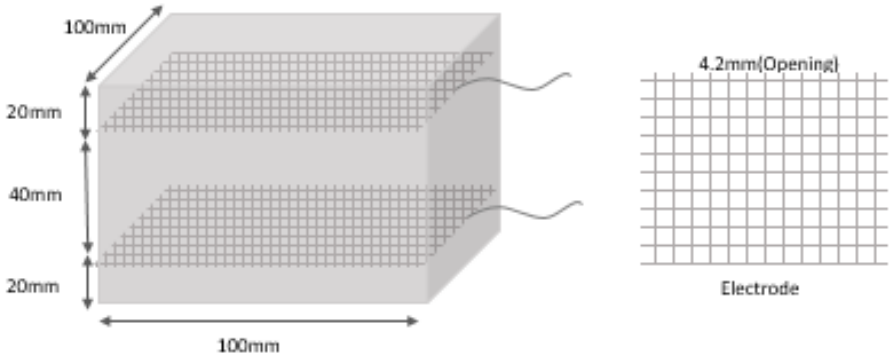

Figure 1. Specimen structure and position of electrodes.

To achieve good sensing and mechanical properties of cement sensor, a new cement composite, hybrid with carbon black (CB) [35] and activated granulated blast furnace slag (pozzolanic material) with 11.9 % FeO content [31] (Table 1) was used as traffic flow detector in this work. Related literature also concludes that GGBFS with an aluminum content of 12 % (Table 2) helps in the development of hydration product (CSH) and leads to compact and crystal microstructure [36–38]. The stress sensing ability of this composite was investigated in the lab as well as on real road test to explore the feasibility of using as a device for traffic flow monitoring.

Table 1. Properties of granulated blast furnace slag.

Item	Unit	Specification	Results
FeO	%	5-13	10.76
Al_2O_3	%	≤ 18	16.72
SiO_2	%	≤ 36	30.93
CaO (Ca^+)	%	≥ 35	39.51
MnO	%	≤ 1.5	0.35
MgO	%	≤ 12	9.44
S	%	≤ 1.3	0.75
TiO_2	%	≤ 4	3.43
Cl	%	≤ 1	0.01
Moisture	%	≤ 0	8.5
Resistivity	Ω-m	–	27
Granulomere (Fineness)	%	≥ 95	99
Insoluble Residue	%	≤ 0.5	0.28
LOI	%	≤ 3	0.2
Strength Grade	Mpa	–	35.5

Table 2. Properties of carbon black.

Items	Unit	Specifications	Results
Carbon particles (C^-)	%	90 Min	93
Apparent Specific Volume	cm^3/g	14~17	16
Iodine Absorption	g/kg	90 Min.	97
HCL Absorption	cm^3/g	3.9 Min.	4.4
Resistivity	Ω, m	3.5 Max.	1.25
Heating Loss	%	0.5 Max.	0.09
Ash	%	0.4 Max.	0.07
Grit	%	0.07 Max.	0.01
Insoluble residue	%	30~35	32

2.2. Preparation of smart cement-based sensor

Initially, an aqueous solution was made by manual stirring of water containing CB and GGBFS along with superplasticizer namely acrylic acid ($C_3H_3O_2Zn^+$) as a water reducing agent. After manual mixing, a probe-type sonicator was used to sonicate the mixture for 15 minutes at a constant nominal frequency of 24 KHz for uniform mixing. A mortar mixer was used for further mixing of the sonicated aqueous solution and other ingredients, i.e. Portland cement, GGBFS, water (0.40 % by weight of binder) for a further 10 minutes. The mixture obtained by mixing machine was then put into the oiled molds with two galvanized mesh electrodes as shown in Fig. 1. Vibrator was used to remove the air voids of the poured mixture. The casted samples were covered with plastic paper to prevent it from the sudden change in atmosphere and then demolded after 24 hours and cured at room temperature for 28 days. Subsequently, the specimens were dried in an oven at 50 ℃ for five days before testing to eliminate the polarization effect due to residue pore water contents. The mix proportions used in this study are mentioned in Table 3.

Table 3. List of specimens and mix proportion.

Specimen Composition	Notation	W/B	Binders		
			CB	GBFS	C
C+CB+GGBFS	**(M1)**	0.40	0.50	5.000	94.5
C+CB+GGBFS	**(M2)**	0.40	1.00	10.00	89.0
C+CB+GGBFS	**(M3)**	0.40	1.50	15.00	83.5
C+CB+GGBFS	**(M4)**	0.40	2.00	20.00	78.0
C+CB+GGBFS	**(M5)**	0.40	2.50	25.00	72.5
C+CB+GGBFS	**(M6)**	0.40	2.50	30.00	67.5

C: Cement, CB: Carbon Black (wt. % of cement), GBFS: Granulated Blast Furnace Slag (wt. % of cement), W/B: water to binder ratio.

2.3. Compressive strength test

Three specimens (50×50×50 mm^3) for each mix proportion were fabricated to investigate the developed compressive strength at 3, 7, 14, 28 days according to standard test method for compressive strength of hydraulic cement using 2 in or 50 mm cube (ASTM C109). Equation-1 can calculate the compressive strength values.

$$\sigma_c = \frac{p}{A} \tag{1}$$

where

σ_c refers to the average compressive strength of three samples (MPa);

P refers to the maximum load applied (N);

A refers to the area of the specimen (mm^2).

2.4. Tensile strength test

To calculate the tensile strength of cement based sensor, three bar-shaped samples of size (40×40×160 mm^3) for each mix design, after being cured at 3, 7, 14 & 28 days were carried out for tensile strength according to ASTM C348. Tensile strength was calculated by Equation-2.

$$\sigma_t = \frac{3FS}{2wh2} \tag{2}$$

where

σ_t refers to the average tensile strength (MPa);

F refers to an applied force by a universal testing machine (N);

S refers to span (mm);

w refers to the width (mm);

h refers to depth (mm).

2.5. Analytical characterizations

Previous studies on utilization of GBFS concluded that higher replacements of this pozzolanic material by cement restart the hydration products at early stages but increased curing age, the hydration production can be comparable to Portland cement [36–38] at curing age of 28 days. In this research work, the development of crystalline (hydrated) and amorphous phases (anhydrate) in cement sensor filled with CB and GBFS, powder X-ray diffraction technique was adopted. The samples were crushed and milled into powder (< 300 μm) at curing age of 28 for XRD testing. Before testing of samples at different curing ages, the further hydration of cement sensor was stopped by washing and repeated immersing in isopropanol for 1 hour. X-ray diffractometer scans the samples between 2θ values of 10° to 60°, and the required data were collected. X´pert high score (version 3) software was used to analyze the received data employing XRD.

The microstructure of cement sensors was observed by employing SEM along with energy EDS (to observe the hydration at a specific point). Isopropanol was used to stop further hydration of samples and dried in the oven at 40 °C. After that, the samples were introduced to the machine (JEOL, EDS DETECTOR manufactured by japan) for SEM/EDS observations.

2.6. Piezoresistivety of cement-based sensors

The laboratory test setup to assess the piezoresistive properties of (28 days cured and dried at 50 °C in the oven for 5 days) smart cement based sensors is described in Fig. 2. All the sensors with different mix designs were tested in the laboratory to check their sensitivity to applied stresses. Electrodes buried in the specimens were energized by UNI-T 30-volt DC supply. Uniaxial repeated compressive loads of 20 KN and 15 KN were applied by universal testing machine. Change in resistance due to applied load was recorded simultaneously by the data acquisition device.

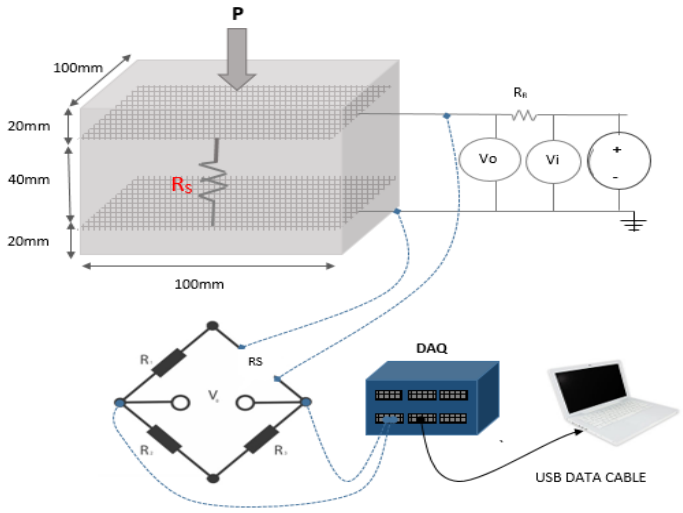

Figure 2. Setup adopted to check the sensitivity of cement sensor to loading.

2.7. Road test

Road test of smart cement sensor was performed in an open environment to observe the feasibility of using it as a device for vehicle detection. A trench was made in pavement and sensor was buried. Cement paste was used to fix the sensor at its place as the vehicles have to pass over it for testing. Vehicles with different axle loads and speed were driven to pass over self-sensing cement sensor in order to investigate its designed sensibility (Fig. 3a and Fig. 3b).

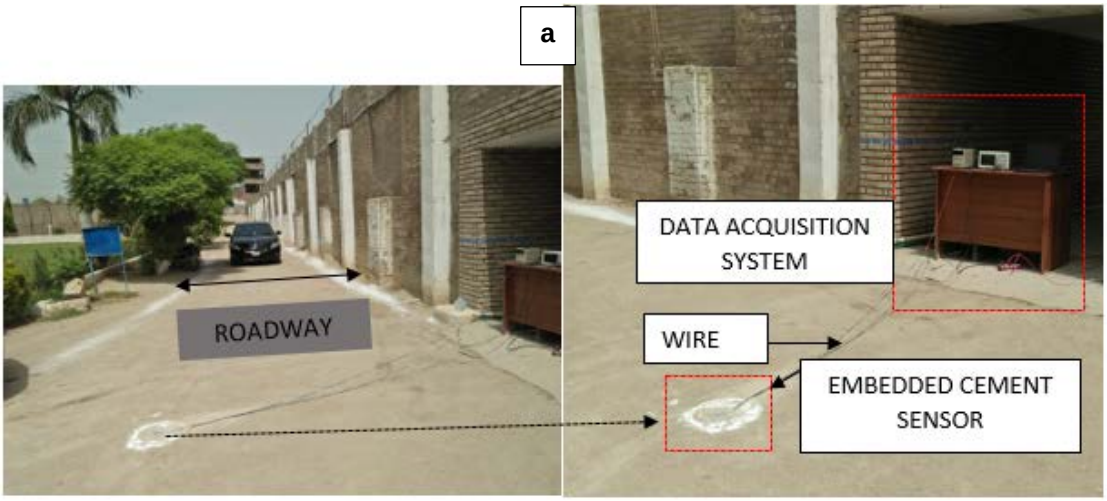

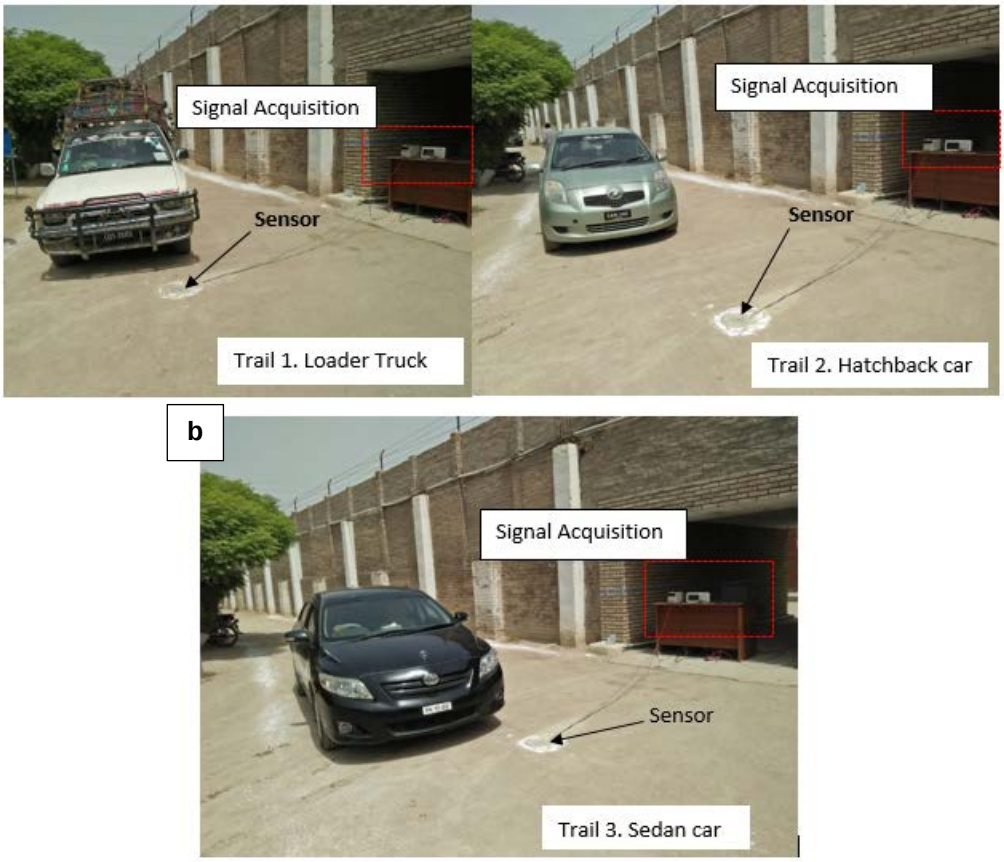

Figure 3. Road Testing (a). Position of embedded sensor and assembly of the data acquisition system, (b). Outdoor testing to check the response of sensor under vehicular loading).

Table 4. List of vehicles passed over cement sensor.

Sr.#	Vehicle type	Weight as per documents (Kg)
01	Hatchback car	1350
02	Sedan car	1600
03	Loader truck	2200

Change in electrical resistivity of cement sensor due to externally applied load denotes the sensing property of self-sensing material and according to Ohm's law (Eq. 3).

$$fs \, \mathrm{X} \frac{L}{A} = Rs \tag{3}$$

where R_s, A, and L refer to the electrical resistivity of the sensor when it was attached to DC power supply, the cross-sectional area of the sensor and the space between two electrodes, respectively.

After passing vehicle over the sensor, the resistance of the sensor will change, and Eq. 3 can be written as Eq. 4.

$$\frac{df_s}{fs} = \frac{dRs}{Rs} - \frac{(1+2\mu)dL}{L} \tag{4}$$

The deformation of the sensor under compressive load is minimal so change in L (dL) can be neglected [39], and Eq. 4 can be modified as Eq. 5.

$$\frac{dRs}{Rs} = \frac{dfs}{fs} \tag{5}$$

It can be observed from Eq. (5) that the change in electrical resistance of the sensors is the same as that of electrical resistivity. Furthermore, Fig. 4 shows a circuit diagram of cement sensor connected in series with constant reference resistance and applied voltage along with the data acquisition process.

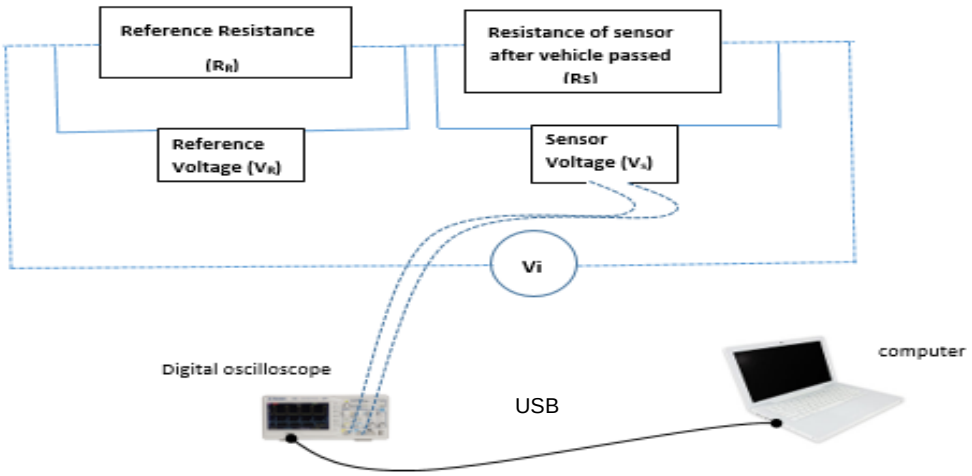

Figure 4. Experimental setup for road testing.

$$\frac{Vs}{Rs} = \frac{Vi - Vs}{RR} \tag{6}$$

Where R_s is the resistance of sensor after the vehicle passes over it and R_R is the reference resistance of sensor before vehicle passing. V_i and V_s are the voltages before and after the application of car load respectively. Eq. (4) can further be written as

$$\frac{Vs}{Vi - Vs} \text{X } RR = Rs \tag{7}$$

The car load made the change in resistance and applied of the sensor which can be expressed as

$$Rs + dRs = \frac{(Vs + dVs)}{Vi - (Vs + dVs)} \text{X } RR \tag{8}$$

Where dV_s change in voltage, and it is much smaller than (V_i–V_s). Thus, Eq. (7) and (8) can be combined and written as

$$\frac{dRs}{Rs} \cong \frac{dVs}{Vs} \tag{9}$$

Eq. (9) clearly shows that change in resistance of cement sensor caused by vehicular loading is approximately equaled to change in applied voltage which is taken as an indication of passing vehicles over the smart cement-based sensor. Digital storage oscilloscope made by UNI-T (UTD20000/3000) was used for real time sampling with the frequency of 250 hz.

3. Results and Discussion

3.1. Compressive strength

The effect of partial replacement of GGBFS and CB by cement on compressive strength is shown in Fig. 5. It can be observed from compressive strength development chart (developed at 3, 7, 14, 28 days) that cement composite named as M4 composed of 2 % CB and 20 % GGBFS shows higher strength at 28 days than other mixes. It is due to the pozzolanic reaction of GGBFS combined with the optimum amount of CB (1 %) to form calcium silicate hydrate (CSH). It can also be noted that the amount of GGBFS and CB beyond M4 causes a slight decrease in compressive strength due to higher accumulation of both the filler in cement composite [36].

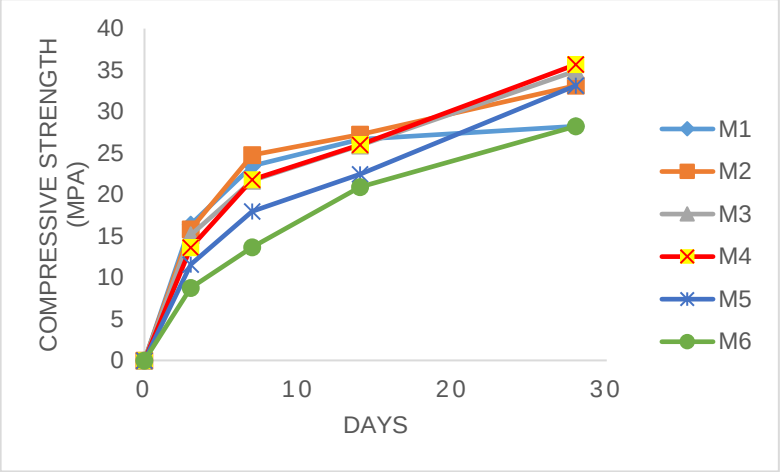

Figure 5. Development compressive strength of cement sensor.

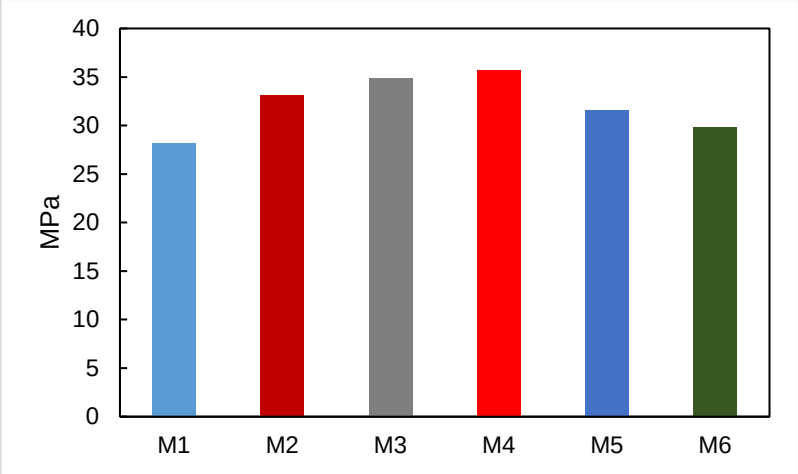

Figure 6. 28 days compressive strength chart.

3.2. Tensile strength

The tensile strength of mortars combined with CB and GGBFS at 3, 7, 14 & 28 days is shown in Fig. 7. A slight increase in tensile strength can be observed for M3 mix as compared to other mixes, but no major change in tensile strength was seen by adding GGBFS and CB. The minor increase in the flexural strength is supposed to be not only from pozzolanic material filling the pores of hydration but also from the tubes linking effect providing support to the matrix which contributes better opposition to stretching effect produced by application of load. It is also noted that the good results will largely depend on proper dispersion of filling material as they would be expected to perform much better regarding the tensile strength of cement-based self-sensing material [15]. In this work, no substantial change in tensile strength is observed compared to plane cement paste.

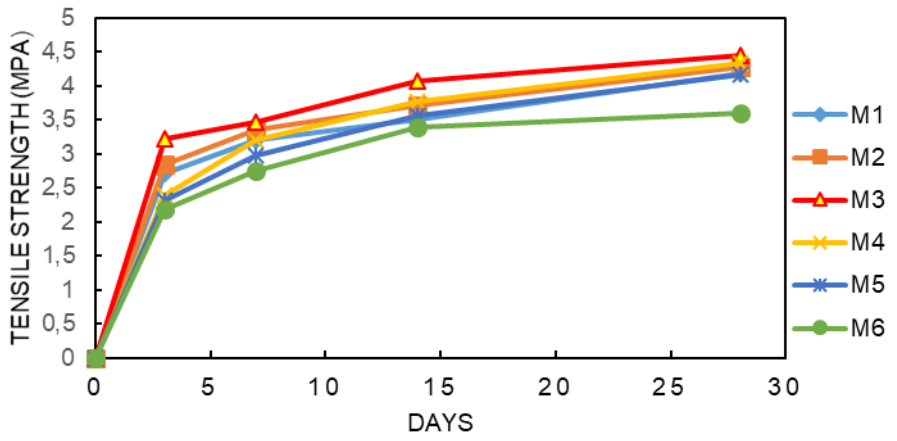

Figure 7. Development tensile strength of cement sensor.

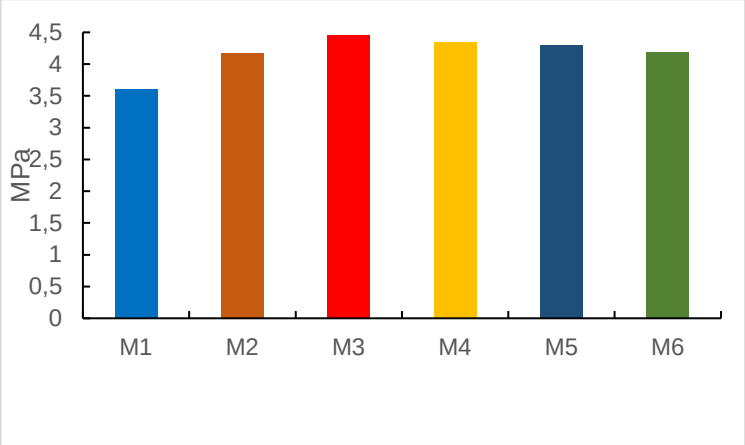

Figure 8. 28 days' tensile strength chart.

3.3. Microstructure

3.3.1 X-ray diffraction (XRD)

Fig. 9 demonstrates the results of XRD analysis of different samples at 3, 7, 14 and 28 days curing. Calcium hydroxide (CH), calcium silicate hydrate (CSH), ettringite, calcium, and quartz are the major hydration products detected by X-ray diffractometer and analyzed by X´pert high score (version 3) software. CH and CSH are the hydration product of alite (C_3S) and belite (C_2S), ettringite is formed by hydration of tri-calcium aluminate (C_3A) and quart by impurities present in binder during the hydration process or curing [40, 41]. It can be noted from Fig. 9(a) and (b) that M1 and M2 show relatively analogous XRD pattern. Approximately identical peaks were observed while comparing the 28 days' results of M3, M4, and M5, M6 that can be observed in Fig. 9(c) to (f).

The peak intensities of all the hydration products at all curing ages in M1 and M2 show no major changes except a decrease in the peak of alite at 2θ value of 33.7° and increase in peak of CH at 2θ value of 29.2° and 46.2° at 28 days curing which is clearly a sign of development of hydration products. Moreover, it was also noted that the peak of ettringite at 14.7° disappears at 28 days curing age which indicates that hydration of tri-calcium aluminate (C3A) is almost completed.

Moreover, at the increase in the filling material into cement, a little change was noted while comparing the XRD of M3 and M4 with M1 and M2. The peak of calcium hydroxide obtained at 2θ value of 19.45° and 46.2° shows no significance at curing age of 3 days because a comparatively high dose of blast furnace slag retards the hydration process at an early age [40]. Furthermore, the peak of ettringite at 2θ value of 14.7° a small peak was noted at 28 days curing age which indicates the slow hydration rate of tri-calcium aluminate (C_3A) due to high accommodation of pozzolanic fillers but interestingly 28 days' hydration of all the mixes (M1, M2, M3, M4) was approximately identical to each other as all the hydration products were detected by X-ray diffractometer.

In the mix designs named as M5 and M6, high replacement of GGBFS by cement alters the hydration process at an early age as shown in Fig. 9(e) & (f). By comparing the XRD patterns of M5 and M6 with previous mix designs, a significant change in hydration was noted. While analyzing the patterns of both M5 and M6, no strong peaks of CH and CSH were noted at 2θ value of 19.45°, 29.3° 46.2° and 30.89° respectively at curing age of 3, 7 and 14 days and much amorphous phase was developed between 15° to 54°. This is due to fact that, the GGBFS particles surrounds the cement components especially C_3S, C_2S and C_3A that slows down the formation process of CH (Porlandite), CSH and ettringite at early age (3, 7 & 14 days) and leads to amorphous phase (non-crystalline phase) in cement mix filled with carbon black (CB) and granulated ground blast furnace slag (GGBFS). On the other hand, samples with 28 days hydration could be comparable (negotiable decrease) to other mixes with relatively low GGBFS as all the hydration products were detected at that curing age.

The contribution of CB to hydration was almost negligible. This is due to the fact that CB is not a mechanical activator (pozzolanic material) and it was filled in cement as a conductive material to increase to the sensitivity of cement mix to load/stress; thus a little contribution of CB to hydration of cement could be neglected.

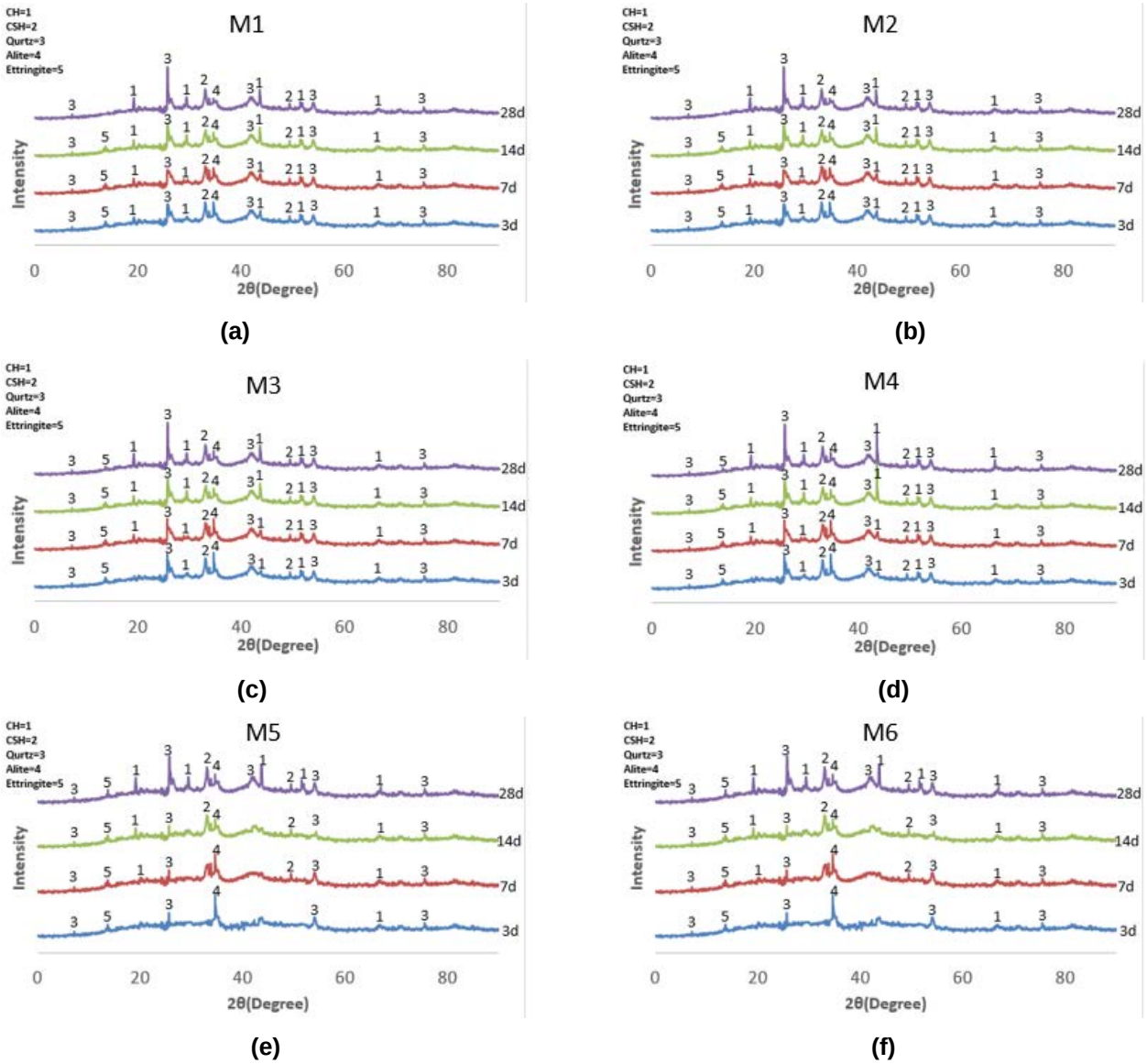

Figure 9. XRD analysis of mix designs at mentioned curing ages.

3.3.2. SEM / EDS

The SEM and EDS were used altogether to detect the microstructure and chemical composition of hydration products of cement paste filled with blast furnace slag and carbon black as pozzolanic conductive materials. The obtained results are shown in Fig. 10 (a) to (c).

It can be observed at 50 µm scale with a very high resolution of × 270, that the paste containing a higher amount of GBFS and CB (M4 and M6) shows dense microstructure as compared to paste with a low amount of both fillers (M1). The filling material specially GBFS ideally covered the pores space between unreacted cement particles and presents a compact and homogenous material because of its excellent pozzolanic reaction with cement. The EDS result of all the three samples show no major difference in the formation of C-S-H gel. The EDS analysis of M1 obtained around unreacted cement shows a Ca/Si ratio of 1.99 which is very much close Ca/Si ratio of plane cement, i.e. 2.02 which indicates the typical C-S-H gel formed by the cement hydration at curing age of 28 days [42, 43]. The EDS of M4 and M6 indicates little decrease in the Ca/Si ratio of 1.81 and 1.68, respectively. This is because of higher accommodation of GBFS and CB in cement which slows down the formation of C-S-H gel and left unreacted particles at 28 days curing age. By analyzing the overall SEM / EDS, the cement paste filled with GBFS and CB as filing material shows excellent and compact microstructure with the excellent chemical composition of hydration product.

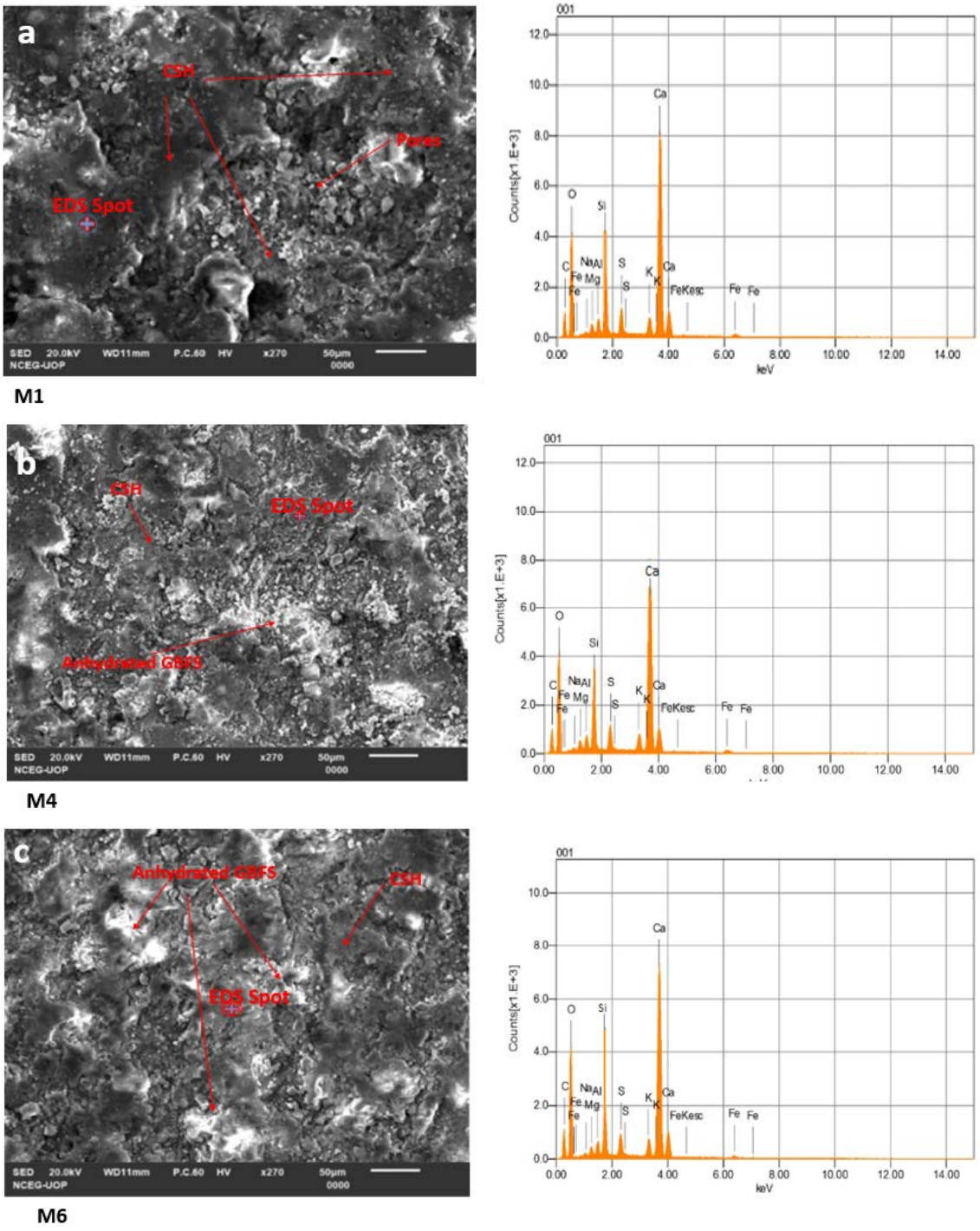

Figure 10. SEM/EDS of mix design M1, M4, and M6.

3.3.3. Piezo-resistive response of self-sensing cement sensor

To find the piezoresistive response of cement sensors, change in electrical resistance was measured in correspondence to applied compressive loads at curing age of 28 days. Cement samples filled with different amount of CB & GGBFS as conductive fillers were put to cyclic compressive loads and the response measured was even and reversible. The results of piezoresistive testing is shown in Fig. 11. It is noted after testing that cement sensor filled with 2.5 % CB and 30 % GGBFS (M6) shows higher sensitivity to applied loading as the relative change in electrical resistivity $d\rho/\rho_o$ (%) reaches about 7.5 % under the compressive load of 15 KN shown in Fig. 7. Thus it can be concluded that CB combined with GGBFS as hybrid filler have great sensing capability when added to cement.

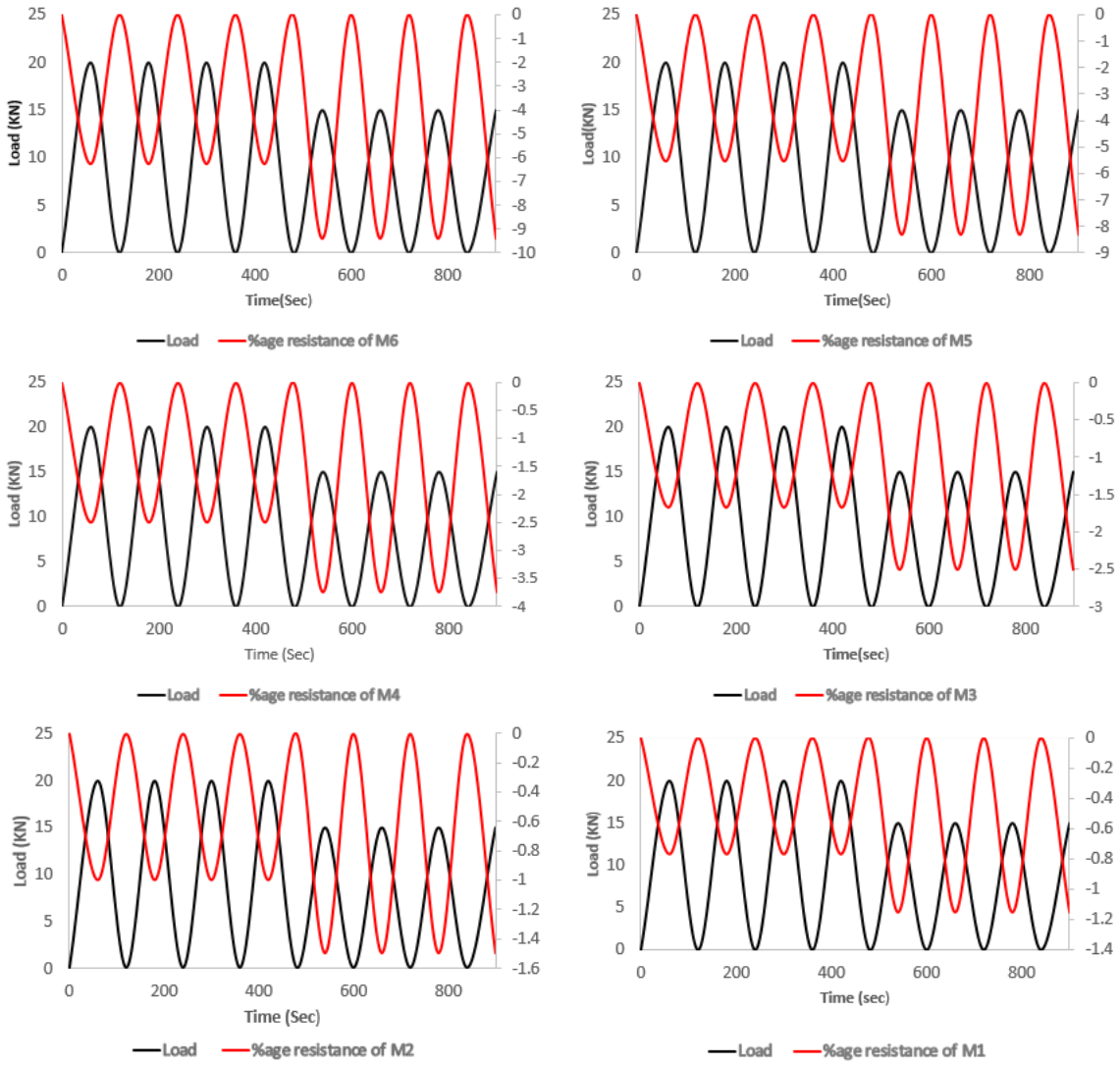

Figure 11. Application of load and a corresponding change in resistance of cement-based sensors filled with different percentages of CB and GGBFS.

Table 5. Maximum percentage resistance of smart sensors in laboratory.

M1 (%)	M2 (%)	M3 (%)	M4 (%)	M5 (%)	M6 (%)
0.933	1.5	2.5	3.75	8.33	9.36

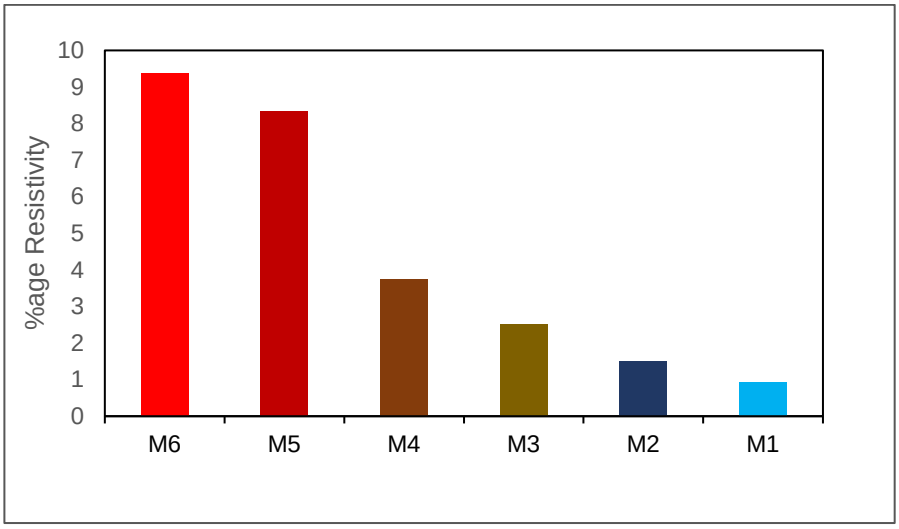

Figure 12. Max percentage resistivity of each sample.

3.3.4. Vehicle detection by cement sensor

Laboratory tests on piezoresistive cement sensors were performed in order to observe their sensitivity and feasibility to use it on the road for vehicle detection. Sensor (M6) which shows maximum sensitivity (i.e., % age change in resistance was maximum to other cement sensors) shown in Fig. 11 (% age resistance of M6) and 12 was adopted for road testing. Different type of vehicles was passed over underneath sensor and the voltage time history record was collected. Sudden change in voltage signals is shown in Fig. 13. Results showed that voltage drop signal was different for a different vehicle which means that the sensor is sensitive to vehicular weight, but the limitation was that one could not measure the exact weight of the vehicle as the position of tyres on cement sensor was different at every trial when a vehicle passes over it. Voltage drop was not uniform even for the same vehicle as axel weight transferred to cement sensor by passing vehicle was not uniform because the contact area between the tyre and cement sensor was not uniform at every trial. Thus, results could be acceptable for vehicle detection, traffic density and vehicle speed as only peak values are required to assess these parameters. Subsequently, this outcome indicates that smart self-sensing cement sensor is feasible to use for detection of passing vehicle as it shows an excellent response in outdoor testing.

Moreover, it was observed that the change in environmental temperature and polarization effect (pore water particles activation due to applied voltage) had an impact on baseline voltage (applied voltage), but the change was continuous and gradual, which did not disturb required results.

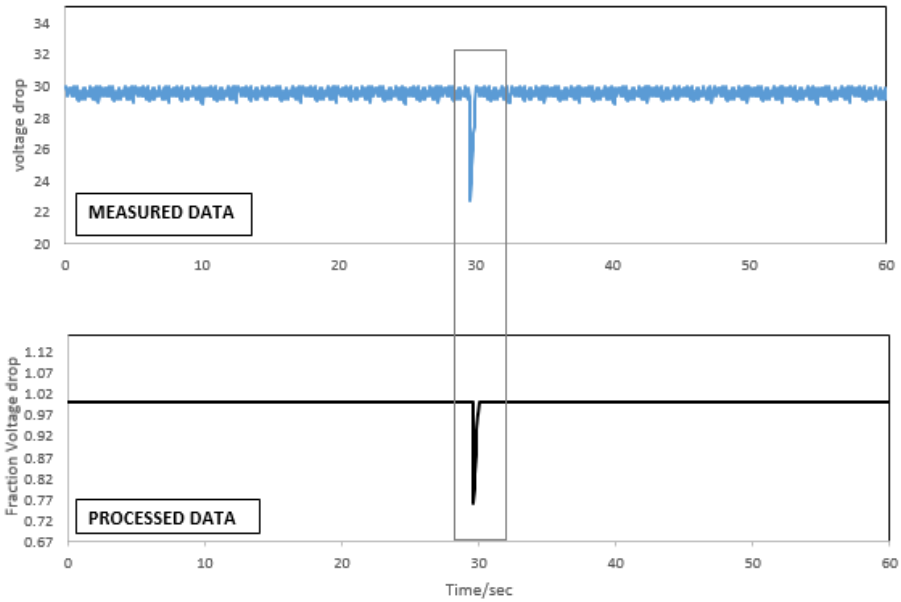

(a). Hatchback passes over cement sensor

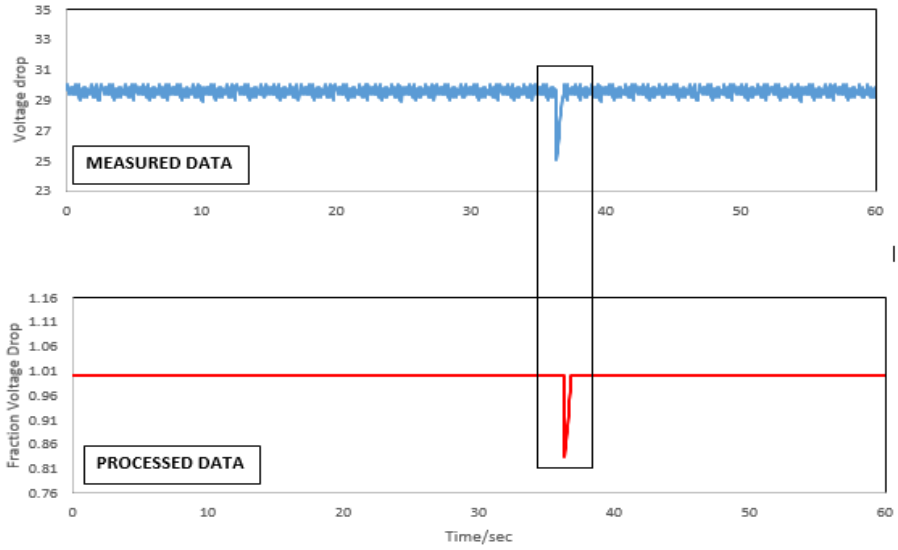

(b). Sedan passes over cement sensor

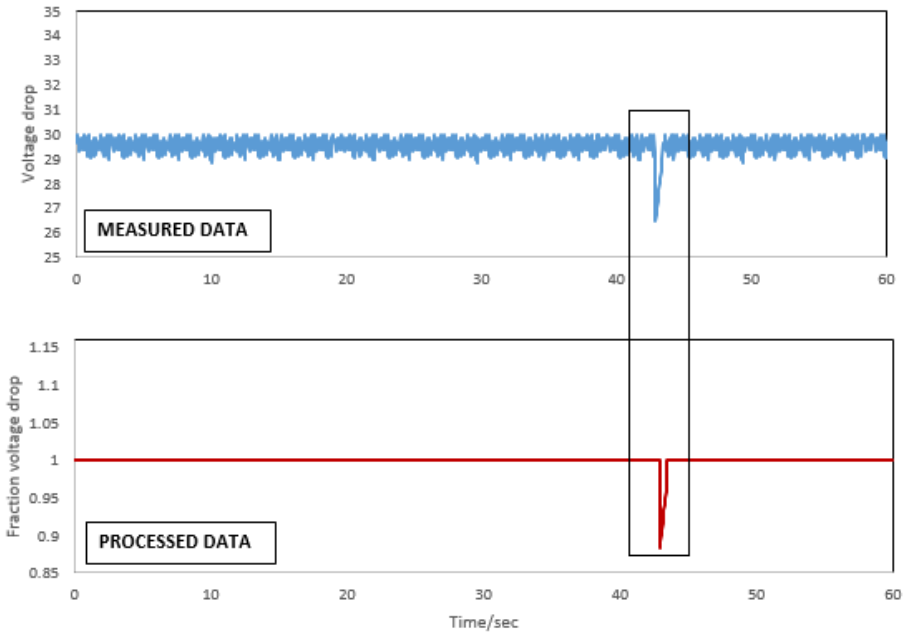

(c). Loader single cabin truck passes over the vehicle

Figure 13. Peak values enclosed in the box shows the passing of different vehicle.

4. Conclusion

Self-sensing CB and GGBFS based cement sensors were fabricated for traffic monitoring. The response was studied for the electrical resistance/electrical voltage of this composite to a repeated compressive load and the vehicular load. The following conclusions are the drawn by the research:

1. The use of GGBFS combined with CB improves both compressive and tensile strength of cement paste due to the pozzolanic reaction and filler effect of GGBFS. Although, CB is a conductive material and does not have pozzolanic properties as compared to GGBFS, but the physical presence of CB resulted in further increase in compressive and tensile strength of cement composite. The optimum improvement for compressive strength is observed at M4 (1 % of CB and 10 % of GGBFS by weight of cement) due to physical filling effect of weak spot and better development of hydration products (CSH and CH) in cement sample but higher percentages of these fillers in cement lead to reduction in compressive strength at early stages because of the existence of extra quantity of filler required for improvement in strength. The improvement in tensile strength can be observed up to 1 % in M3 compared to plane cement paste. It must be noted that tensile strength would largely depend on the dispersion of both the fillers especially GGBFS.

2. The incorporation of GGBFS in cement enhance the hydration products formation compared to plane cement paste [36] at the same curing age but negotiable defect noted was that high (30 %) replacement of GGBFS by cement, retardation/slowdown of hydration process was noted at early age curing, but the later hydration shows no major difference in hydration.

3. SEM/EDS data show that use of GBFS as a pozzolanic filler improves the microstructure of cement paste along with good chemical composition, but it slows down the early age hydration to some extent.

4. Laboratory test to investigate the sensing capability of the cement sensor indicates that there is a corresponding excellent relation between applied compressive load and electrical resistivity and can be used on the road for vehicle detection.

5. The real road test cement sensor also provides an outstanding response to vehicular loading by showing an abrupt/sudden change in baseline voltage.

In conclusion, the findings in lab and road tests indicate that the designed cement sensor has great potential to use as a device for traffic monitoring such as vehicle detection. Moreover, self-sensing cement composite has many advantages including good compatibility with pavement structure, long service life, easy installation and low maintenance cost along with excellent mechanical and microstructural properties.

5. Acknowledgements

The authors acknowledge the technical support given by the Jouf University, Saudi Arabia and Qurtuba University of Science and IT, Dera Ismail Khan, Pakistan, and also acknowledge Dr. Muhammad Waseem (Center of Excellence in Geology, University of Peshawar), Mr. Raheel Khan (Lecturer, EED, QUIST), Mr. Sohail Khalid (EED, QUIST) for providing complimentary technical support in dealing with Telescopic Microscopy (TM) and Probe Sonicator.

References

1. Chong, K.P., Carino, N.J., Washer, G. Health monitoring of civil infrastructures. Proc. SPIE 4337, Health Monitoring and Management of Civil Infrastructure Systems. 2001. URL: https://doi.org/10.1117/12.435595 (date of application: 23.11.2019).
2. Faouzi, N.E., El Klein, L.A. Data Fusion for ITS: Techniques and Research Needs. Transportation Research Procedia. 2016. Pp. 495–512. DOI: 10.1016/j.trpro.2016.06.042
3. Lawrence, A. Klein, Mills, M.K., Gibson, D.R.P. Traffic Detector Handbook: 3rd edn. US Department of Transportation. VA, (October) 2006. 1–16 p.
4. Jelušić, N., Anžek, M., Mandzuka, S. Evaluation of sensor technologies for intelligent transport systems 16th ITS World Congress. 2009. URL: https://bib.irb.hr/datoteka/428217.3931.pdf (date of application 29 July 2019).
5. Han, B., Ou, J. Embedded piezoresistive cement-based stress/strain sensor. Sensors and Actuators, A: Physical. 2007. Pp. 294–29. DOI: 10.1016/j.sna.2007.05.011
6. Shi, Z.Q., Chung, D.D.L. Carbon fiber-reinforced concrete for traffic monitoring and weighing in motion. Cement and Concrete Research. 1999. 29(3). Pp. 435–439. DOI: 10.1016/S0008-8846(98)00204-X
7. Chen, B., Liu, J. Damage in carbon fiber-reinforced concrete, monitored by both electrical resistance measurement and acoustic emission analysis. Construction and Building Materials. 2008. 22(11). Pp. 2196–2201. DOI: 10.1016/j.conbuild-mat.2007.08.004
8. Bontea, D.M., Chung, D.D.L., Lee, G.C. Damage in carbon fiber-reinforced concrete, monitored by electrical resistance measurement. Cement and Concrete Research. 2000. 30(4). Pp. 651–659. DOI: 10.1016/S0008-8846(00)00204-0
9. Han, B., Yu, X., Kwon, E. A self-sensing carbon nanotube/cement composite for traffic monitoring. Nanotechnology. 2009. 20(44). Pp. 445501. DOI: 10.1088/0957-4484/20/44/445501
10. Konsta-Gdoutos, M.S., Aza, C.A. Self sensing carbon nanotube (CNT) and nanofiber (CNF) cementitious composites for real time damage assessment in smart structures. Cement and Concrete Composites. 2014. 53. Pp. 162–169. DOI: 10.1016/j.cemconcomp.2014.07.003
11. Chen, P.W., Chung, D.D.L. Carbon fiber reinforced concrete for smart structures capable of non-destructive flaw detection. Smart Materials and Structures. 1993. 2(1). Pp. 22–30. DOI: 10.1088/0964-1726/2/1/004
12. Wen, S., Chung, D.D.L. Effects of strain and damage on strain-sensing ability of carbon fiber cement. Journal of Materials in Civil Engineering. 2006. 18(3). Pp. 355–360. DOI: 10.1061/(ASCE)0899-1561(2006)18:3(355)
13. Urkhanova, L.A., Buyantuev, S.L., Urkhanova, A.A., Lkhasaranov, S.A., Ardashova, G.R., Fediuk, R.S., Svintsov, A.P., Ivanov, I.A. Mechanical and electrical properties of concrete modified by carbon nanoparticles. Magazine of Civil Engineering. 2019. 92(8). Pp. 163–172. DOI: 10.18720/MCE.92.14
14. Han, B., Guan, X., Ou, J. Electrode design, measuring method and data acquisition system of carbon fiber cement paste piezoresistive sensors. Sensors and Actuators, A: Physical. 2007. 135(2). Pp. 360–369. DOI: 10.1016/j.sna.2006.08.003
15. Wen, S., Chung, D. Strain-Sensing Characteristics of Carbon Fiber-Reinforced Cement. American Concrete Institute Materials Journal.2005. 102(4). Pp. 244–248. DOI: 10.14359/14617
16. Sun, M.Q., Liew, R.J.Y., Zhang, M.H., Li, W. Development of cement-based strain sensor for health monitoring of ultra high strength concrete. Construction and Building Materials. 2014. 65. Pp. 630–637. DOI: 10.1016/j.conbuildmat.2014.04.105
17. Banthia, N., Djeridane, S., Pigeon, M. Electrical resistivity of carbon and steel micro-fiber reinforced cements. Cement and Concrete Research. 1992. 22(5). Pp. 804–814. DOI: 10.1016/0008-8846(92)90104-4
18. Teomete, E. Transverse strain sensitivity of steel fiber reinforced cement composites tested by compression and split tensile tests. Construction and Building Materials. 2014. 55. Pp. 136–145. DOI: 10.1016/j.conbuildmat.2014.01.016
19. Azhari, F., Banthia, N. Cement-based sensors with carbon fibers and carbon nanotubes for piezoresistive sensing. Cement and Concrete Composites. 2012. 34(7). Pp. 866–873. DOI: 10.1016/j.cemconcomp.2012.04.007
20. Li, G.Y., Wang, P.M., Zhao, X. Pressure-sensitive properties and microstructure of carbon nanotube reinforced cement composites. Cement and Concrete Composites. 2007. 29(5). Pp. 377–382. DOI: 10.1016/j.cemconcomp.2006.12.011
21. D'Alessandro, A., Rallini, M., Ubertini, F., Materazzi, A.L., Kenny, J.M. Investigations on scalable fabrication procedures for self-sensing carbon nanotube cement-matrix composites for SHM applications. Cement and Concrete Composites. 2016. 65. Pp. 200–213. DOI: 10.1016/j.cemconcomp.2015.11.001
22. Li, H., Xiao, H. gang, Ou, J. ping. Effect of compressive strain on electrical resistivity of carbon black-filled cement-based composites. Cement and Concrete Composites. 2006. 28(9). Pp. 824–828. DOI: 10.1016/j.cemconcomp.2006.05.004
23. Monteiro, A.O., Cachim, P.B., Costa, P.M.F.J. Electrical Properties of Cement-based Composites Containing Carbon Black Particles. Materials Today: Proceedings. 2015. Pp. 193–199. DOI: 10.1016/j.matpr.2015.04.021
24. Ding, Y., Chen, Z., Han, Z., Zhang, Y., Pacheco-Torgal, F. Nano-carbon black and carbon fiber as conductive materials for the diagnosing of the damage of concrete beam. Construction and Building Materials. 2013. 43, Pp. 233–241. DOI: 10.1016/j.conbuildmat.2013.02.010
25. Wen, S., Chung, D.D.L. Partial replacement of carbon fiber by carbon black in multifunctional cement-matrix composites. Carbon. 2007. 45(3). Pp. 505–513. DOI: 10.1016/j.carbon.2006.10.024
26. Rhee, I., Lee, J.S., Kim, Y.A., Kim, J.H., Kim, J.H. Electrically conductive cement mortar: Incorporating rice husk-derived high-surface-area graphene. Construction and Building Materials. 2016. 125. Pp. 632–642. DOI: 10.1016/j.conbuildmat.20-16.0-8.089
27. Metaxa, Z.S. Exfoliated graphene nanoplatelet cement-based nanocomposites as piezoresistive sensors: influence of nanoreinforcement lateral size on monitoring capability. Ciencia e Tecnologia dos Materiais. 2016. 28(1). Pp. 73–79. DOI: 10.1016/j.ctmat.2015.12.001

28. Lee, S.J., You, I., Zi, G., Yoo, D.Y. Experimental investigation of the piezoresistive properties of cement composites with hybrid carbon fibers and nanotubes. Sensors (Switzerland). 2017. 17(11). P. 2516. DOI: 10.3390/s17112516
29. Han, B.G., Han, B.Z., Ou, J.P. Novel piezoresistive composite with high sensitivity to stress/strain. Materials Science and Technology. 2010. 26(7). Pp. 865–870. DOI: 10.1179/026708309X12454008169546
30. Zhang, J., Lu, Y., Lu, Z., Liu, C., Sun, G., Li, Z. A new smart traffic monitoring method using embedded cement-based piezoelectric sensors. Smart Materials and Structures. 2015. 24(2). P. 25023. DOI: 10.1088/0964-1726/24/2/025023
31. Jia, X., Zhang, Y., Qian, J. Compression sensibility of magnetic-concentrated fly ash mortar under uniaxial loading. Journal Wuhan University of Technology, Materials Science Edition. 2012. 27(5). Pp. 999–1003. DOI: 10.1007/s11595-012-0588-y
32. Monteiro, A.O., Cachim, P.B., Costa, P.M.F.J. Self-sensing piezoresistive cement composite loaded with carbon black particles. Cement and Concrete Composites. 2017. 81, Pp. 59–65. DOI:10.1016/j.cemconcomp.2017.04.009
33. Han, B., Zhang, L., Sun, S., Yu, X., Dong, X., Wu, T., Ou, J. Electrostatic self-assembled carbon nanotube/nano carbon black composite fillers reinforced cement-based materials with multifunctionality. Composites Part A: Applied Science and Manufacturing, 2015.79. Pp. 103–115. DOI: 10.1016/j.compositesa.2015.09.016
34. Ji, M., Mason, M., Modarelli, D., Parquette, J. Threading carbon nanotubes through a self-assembled nanotube. Chemical Science.2019. 10(34), Pp. 7868–7877. DOI: 10.1039/c9sc02313e
35. Chung, D.D.L. Carbon materials for structural self-sensing, electromagnetic shielding and thermal interfacing. Carbon. 2012. 154, Pp. 1079–1086. DOI: 10.1016/j.carbon.2012.01.031
36. Monteiro, A.O., Loredo, A., Costa, P.M.F.J., Oeser, M., Cachim, P.B. A pressure-sensitive carbon black cement composite for traffic monitoring. Construction and Building Materials. 2017. 154, Pp. 1079–1086. DOI: 10.1016/j.conbuildmat.2017.08.053
37. Kumar, S., Kumar, R., Bandopadhyay, A., Alex, T.C., Ravi Kumar, B., Das, S.K., Mehrotra, S.P. Mechanical activation of granulated blast furnace slag and its effect on the properties and structure of portland slag cement. Cement and Concrete Composites. 2008. 30(8). Pp. 679–685. DOI: 10.1016/j.cemconcomp.2008.05.005
38. Ben Haha, M., Le Saout, G., Winnefeld, F., Lothenbach, B. Influence of activator type on hydration kinetics, hydrate assemblage and microstructural development of alkali activated blast-furnace slags. Cement and Concrete Research. 2011. 41(3). Pp. 301–310. DOI: 10.1016/j.cemconres.2010.11.016
39. Liu, G., Florea, M.V.A., Brouwers, H.J.H. The hydration and microstructure characteristics of cement pastes with high volume organic-contaminated waste glass powder. Construction and Building Materials. 2018. 87. Pp. 1177–1189. DOI: 10.1016/j.conbuildmat.2018.07.162
40. Han, B., Zhang, K., Yu, X., Kwon, E., Ou, J. Nickel particle-based self-sensing pavement for vehicle detection. Measurement: Journal of the International Measurement Confederation. 2011. 44(9). Pp. 1645–1650. DOI: 10.1016/j.measurement.20-11.06.014
41. Slavchevaa, G., Khanb, M., Baidzhanovb, D., Shvedovac, M., Imanovb, Y. (2019). Slinkerless slag-silica binder: hydration process and hardening kinetics. Magazine of Civil Engineering. 2019. 92(8). Pp. 96–105. DOI: 10.18720/MCE.92.8
42. Rodger, S.A., Groves, G.W. Electron Microscopy Study of Ordinary Portland Cement and Ordinary Portland Cement–Pulverized Fuel Ash Blended Pastes. Journal of the American Ceramic Society. 1989. 72(6). Pp. 1037–1039. DOI: 10.1111/j.1151-2916.1989.tb06265.x
43. Richardson, I.G., Groves, G.W. Microstructure and microanalysis of hardened ordinary Portland cement pastes. Journal of Materials Science. 1993. 28(1). Pp. 265–277. DOI: 10.1007/BF00349061

Contacts:

Muhmmad Tariq Bashir, tariqbashir@cecos.edu.pk

Muhmmad Daniyal, drmtb@qurtuba.edu.pk

Majed Alzara, arc_majed@hotmail.com

Mahmoud Elkady, m.s.h.kady@gmail.com

Ammar Armghan, aarmghan@ju.edu.sa